Pacific decadal oscillation influences tropical oxygen minimum zone extent and obscures anthropogenic changes.

Mathieu Poupon[1], Laure Resplandy[1], Marina Lévy[2], and Laurent Bopp[3]
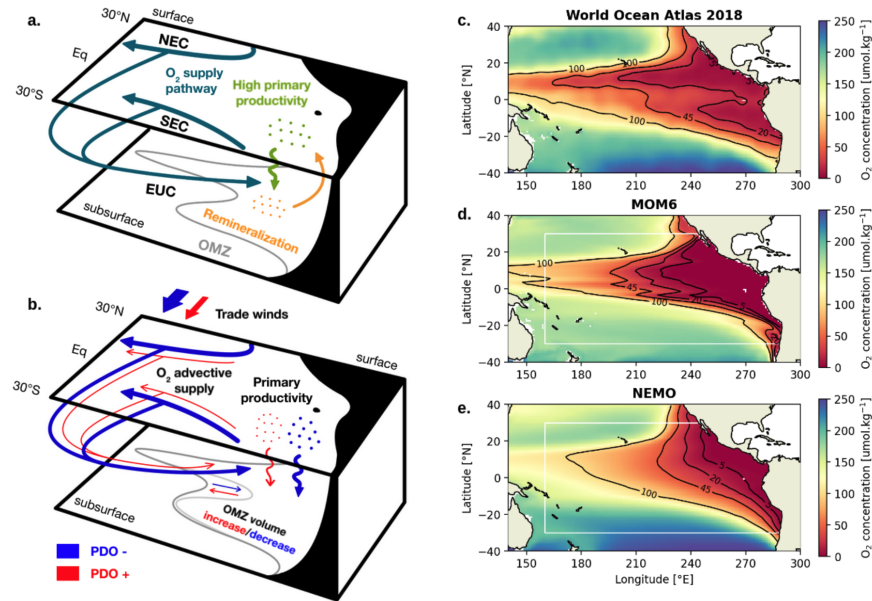
[1]Princeton University
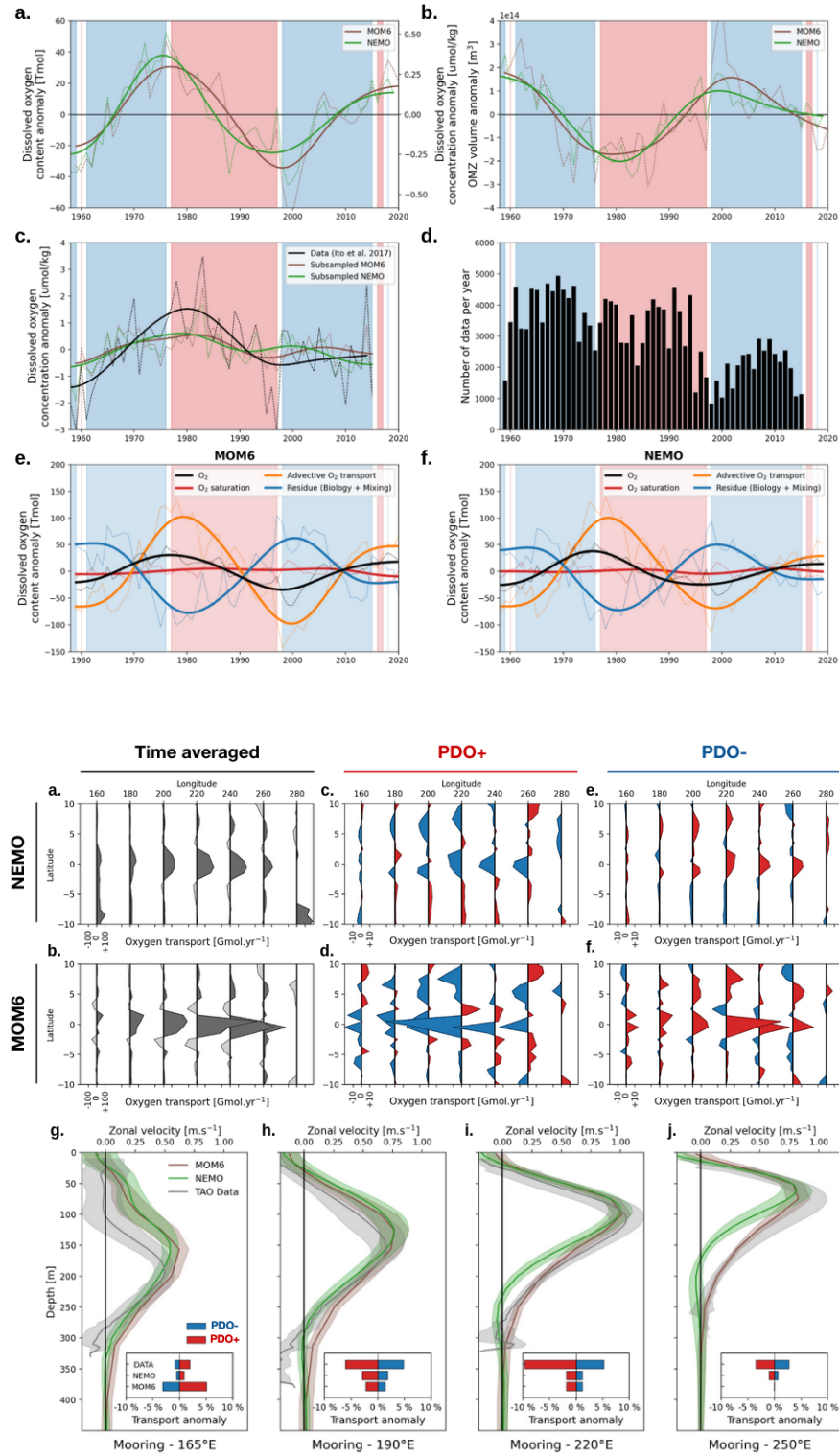[2]LOCEAN-IPSL, CNRS/UPMC/IRD/MNHN
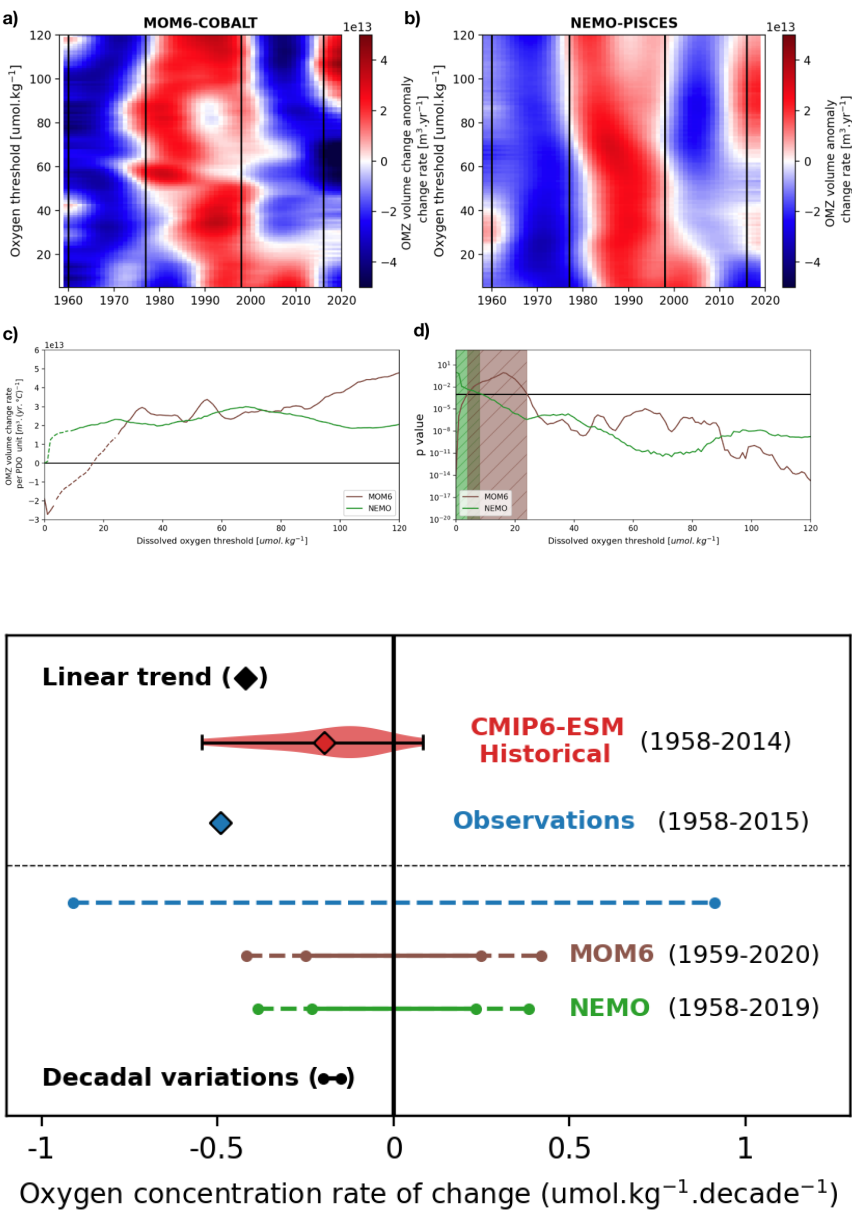[3]LSCE-IPSL, CNRS/CEA/UVSQ

December 7, 2022

Abstract

Observations suggest that the tropical Pacific Ocean has lost oxygen since the 1960s leading to the expansion of its oxygen minimum zone (OMZ). Attribution to anthropogenic forcing is, however, difficult because of limited data availability and the large natural variability introduced by the Pacific Decadal Oscillation (PDO). Here, we evaluate the PDO influence on oxygen dynamics and OMZ extent using observations and hindcast simulations from two global ocean circulation models (NEMO-PISCES, MOM6-COBALT). In both models, the tropical Pacific oxygen content decreases by about 30 Tmol.decade^{-1} and the OMZ volume expands by 1.3×10^5 km^3.decade^{-1} during PDO positive phases, while variations of similar magnitude but opposite sign are simulated during negative phases. Changes in equatorial advective oxygen supply, partially offset by biological demand, control the oxygen response to PDO. Observations which cover 39\% of the tropical Pacific volume only partially capture spatio-temporal variability, hindering the separation of anthropogenic trend from natural variations.

1

2

Pacific decadal oscillation influences tropical oxygen minimum zone extent and obscures anthropogenic changes.

Mathieu A. Poupon[1,2], Laure Resplandy[1,3], Marina Lévy[4], Laurent Bopp[5]

[1]Department of Geosciences, Princeton University, Princeton, NJ, USA
[2]Atmospheric and Oceanic Sciences Program, Princeton University, Princeton, NJ, USA
[3]High Meadows Environmental Institute, Princeton University, Princeton, NJ, USA
[4]LOCEAN-IPSL, CNRS, Sorbonne Université, Paris, France
[5]LMD-IPSL, CNRS-ENS-UPMC-X, Paris, France

Key Points:

- PDO modulates tropical Pacific oxygen content and OMZ volume on decadal time scales.
- The PDO-induced variations are of the same order of magnitude as the anthropogenic deoxygenation signal.
- Currently available data are too sparse to resolve and isolate the PDO-induced and anthropogenic signals.

Corresponding author: Mathieu A. Poupon, `mpoupon@princeton.edu`

Abstract

Observations suggest that the tropical Pacific Ocean has lost oxygen since the 1960s leading to the expansion of its oxygen minimum zone (OMZ). Attribution to anthropogenic forcing is, however, difficult because of limited data availability and the large natural variability introduced by the Pacific Decadal Oscillation (PDO). Here, we evaluate the PDO influence on oxygen dynamics and OMZ extent using observations and hindcast simulations from two global ocean circulation models (NEMO-PISCES, MOM6-COBALT). In both models, the tropical Pacific oxygen content decreases by about 30 Tmol.decade^{-1} and the OMZ volume expands by 1.3×10^5 km^3.decade^{-1} during PDO positive phases, while variations of similar magnitude but opposite sign are simulated during negative phases. Changes in equatorial advective oxygen supply, partially offset by biological demand, control the oxygen response to PDO. Observations which cover 39% of the tropical Pacific volume only partially capture spatio-temporal variability, hindering the separation of anthropogenic trend from natural variations.

Plain Language Summary

Human activities cause oxygen loss in the ocean, which leads to the expansion of areas with very low oxygen concentrations located in the tropics called oxygen minimum zones (OMZ). Understanding the dynamics of OMZs is crucial because they produce greenhouse gasses and are unsuitable for the life of most large marine organisms. Quantifying the response of OMZs is however complicated by natural variability that superimposes on human-induced changes. In the Pacific Ocean, one of the strongest natural variability phenomena is the Pacific Decadal Oscillation (PDO). We used data and numerical models to assess the magnitude of oxygen changes caused by this natural phenomena in the tropical Pacific Ocean, and show that they are comparable to that of human-induced oxygen changes. We highlight that more oxygen data is needed to accurately separate natural variations from human-induced changes, and that a fraction of the oxygen loss attributed to human activities in prior work could in fact be due to natural variability.

1 Introduction

Since 1960, the ocean has lost 1 to 2% of its global oxygen content (Helm et al., 2011; Ito et al., 2017; Schmidtko et al., 2017). In the tropical Pacific, in situ observations suggest that the deoxygenation rate is between -0.1 and -0.3 umol.kg^{-1}.yr^{-1} (30°N-30°S in upper 1000 m, Helm et al., 2011; Stramma et al., 2012; Long, Deutsch, & Ito, 2016; Ito et al., 2017; Schmidtko et al., 2017), and Earth system models project that it will continue during the 21st century at a rate ranging from -0.05 to -0.1 umol.kg^{-1}.yr^{-1} if emissions are not curtailed (i.e. under high emission scenarios, Bopp et al., 2013; Bopp, Resplandy, Untersee, Le Mezo, & Kageyama, 2017; Long et al., 2016; Levin, 2018; Oschlies et al., 2017; Kwiatkowski et al., 2020). The tropical Pacific hosts the world's largest oxygen minimum zone (OMZ), which has likely expanded in response to this substantial deoxygenation (Stramma et al., 2008; Keeling et al., 2010; Helm et al., 2011; Ito et al., 2017; Schmidtko et al., 2017). Deoxygenation is particularly critical near OMZs since the expansion of their volume threatens ecosystems by reducing niches of many macro-organisms such as tunas and marlins (Vaquer-Sunyer & Duarte, 2008; Stramma et al., 2010, 2012; Breitburg et al., 2018), and affects the production of nitrous oxide, a potent greenhouse gas (Babbin et al., 2015; Yang et al., 2020). While global deoxygenation is unambiguously attributed to anthropogenic warming, it is still unclear to which extent changes in the tropical Pacific OMZ volume are obscured by natural variability (Ito & Deutsch, 2010; Deutsch et al., 2014; Long et al., 2016; Oschlies et al., 2017; Ito et al., 2019; Busecke et al., 2019), partly because oxygen data are relatively sparse and sampling has been heterogeneous in this region over the last decades. (Ito et al., 2017).

The Pacific Decadal Oscillation (PDO, Mantua, Hare, Zhang, Wallace, & Francis, 1997) is a major source of oxygen natural variability in the tropical Pacific on decadal time-scales (Duteil et al., 2018; Ito et al., 2019). Oxygen concentrations at the subsurface, where the OMZ is located, are controlled by the balance between biological demand and physical supply by the subtropical cells and the equatorial undercurrent (Figure 1a, e.g., Brandt et al., 2015; Busecke et al., 2019). The PDO modulates both the physical and the biological processes that control oxygen supply and consumption. During positive phases, trade winds slacken, causing a slowdown of subtropical cells (Hong et al., 2014) and the associated oxygen supply to the subsurface tropical Pacific (Duteil et al., 2014, 2018; Ito et al., 2019), while the vertical movement of isopycnals deepens the eastern tropical oxycline (Ito et al., 2019) as well as the thermocline leading to reduced respiration and oxygen demand (Deutsch et al., 2011, 2014). Negative phases are associated with the opposed response, including a more vigorous oxygen supply by subtropical cells and increased oxygen demand. Duteil and co-authors showed that circulation changes exceeded biological changes and that the OMZ volume was larger in an idealized ocean model experiment of perpetual positive PDO than in a companion experiment of perpetual negative PDO (Duteil et al., 2018).While these idealized experiments have clearly shown that the PDO has potential to induce significant OMZ volume changes, the magnitude of variations caused by a realistic PDO, which switches phase on decadal time scales and how it affects our ability to estimate and attribute the anthropogenic trend, has not been estimated yet.

Here we use two biophysical hindcast simulations reproducing the PDO's historical oscillations and an oxygen data product (Ito et al., 2017) both covering the past ~60 years to study and quantify the PDO impact on oxygen dynamics in the tropical Pacific. First, we show that PDO-induced changes in oxygen content and OMZ volume are of the same order of magnitude as those previously attributed to anthropogenic climate change. We find that the poor spatial and temporal observation coverage in this region does not allow to resolve these natural decadal variations, nor to attribute long-term trends. Finally we identify the mechanisms responsible for these variations.

2 Methods

2.1 Two ocean biophysical models

We used hindcast simulations from two ocean biophysical models: i) the Modular Ocean Model version 6 (MOM6, Adcroft et al. (2019)) coupled with the Carbon, Ocean Biogeochemistry and Lower Trophics biogeochemical module version 2 (COBALT, Stock et al. (2020)) developed by the Geophysical Fluid Dynamics Laboratory (GFDL), and ii) the Nucleus for European Modelling of the Ocean version 3.6 (NEMO, Madec et al. (2017)) coupled with the Pelagic Interactions Scheme for Carbon and Ecosystem Studies biogeochemical module version 2 (PISCES-v2, Aumont et al. (2015)) developed by the Institute Pierre-Simon Laplace (IPSL). COBALT and PISCES are intermediate complexity biogeochemical modules including 33 and 24 state variables respectively (e.g., 3 and 2 phytoplanktons, 3 and 2 zooplanktons, and nutrients such as nitrogen, phosphorus, iron and silica). The nominal horizontal resolution is 0.5° for MOM6 (i.e., 0.5° in longitude and 0.25° in latitude at the equator increasing to 0.45° at 30°N-30°S) and 1° for NEMO (1° in longitude and 0.3° in latitude at the equator increasing to 1° at 30°N-30°S). Both simulations are forced by the Japanese atmospheric reanalysis products (JRA55-do version 1.3 and 1.4, Tsujino et al. (2018) for MOM6 and NEMO, respectively). MOM6 was run for 1959-2020 after a 81 years spin up (see details in Liao et al. (2020)) and NEMO was run for 1958-2019 after a 122 years spin up (see details in Friedlingstein et al. (2020)). Results are presented for the upper tropical Pacific (0-1000m, 30°S-30°N, 160°E-eastern coast, see white box in Figure 1d,e). We removed the 62-year deoxygenation and OMZ expansion trends (associated with processes with periods greater than the PDO, such as model drift or anthropogenic forcing) from the oxygen concentration (-45 Tmol.decade^{-1}

in NEMO, -10 Tmol.decade^{-1} in MOM6) and OMZ volume ($+5.6\times10^{14}$ m^3.decade^{-1} in NEMO, $+9.7\times10^{14}$ m^3.decade^{-1} in MOM6) time-series in both simulations.

The MOM6 and NEMO simulations represent the main features of the Pacific oxygen minimum zone (Figure 1c,d,e). including the horizontal footprint of the volume delimited by the 45 umol.kg^{-1} oxygen isoconcentration extending from 20°S to 39°N and from 220°E to the American continent at the equator. Simulated oxygen fields in the upper tropical Pacific (0-1000m, 30°S-30°N, 160°E-eastern coast, see white box in Figure 1d,e) have an average RMSE of 18.3 umol.kg^{-1} in MOM6 and 20.3 umol.kg^{-1} in NEMO compared to the World Ocean Atlas 2018 (WOA18) oxygen concentration climatology. Notable biases are a factor of two overestimation of the suboxic volume (< 20 umol.kg^{-1}) in MOM6 (17.6×10^{15} m^3, vs. 8.6×10^{15} m^3 in WOA18 and 9.0×10^{15} m^3 in NEMO), and a poor representation of the Equatorial undercurrent (EUC), and off-equatorial alternating jets which prevent the separation of the equatorial OMZ into a northern and southern lobe in NEMO (Figure 1c,d,e).

2.2 Observational data

We use the oxygen data product created by Ito et al. (2017) covering the upper 1000m of the ocean over the period 1958-2015 to estimate the amplitude of decadal variations in observations. We use data from four tropical ocean atmosphere (TAO) moorings collected monthly at the equator (0°N) almost continuously from 1988 to the present at longitudes: 165°E, 190°E, 220°E, 250°E and distributed by NOAA (https://www.pmel.noaa.gov/gtmba/) to evaluate the simulated meridional velocity in the two models. We also used oxygen data from the World Ocean Atlas 2018 (WOA18, (Garcia et al., 2019)) available online to evaluate the simulations.

2.3 Earth System Model Ensemble

We used the oxygen fields produced by 14 latest generation Earth system models from the Coupled Model Intercomparison Project Phase 6 (CMIP6, Eyring et al. (2016)). Namely we use the following models: ACCESS-ESM1-5, CNRM-ESM2-1, CanESM5-CanOE, CanESM5, GFDL-CM4, GFDL-ESM4, IPSL-CM6A-LR,MIROC-ES2L, MPI-ESM1-2-HR, MPI-ESM1-2-LR, MRI-ESM2-0, NorESM2-LM, NorESM2-MM, UKESM1-0-LL. The linear trend in dissolved oxygen contained in the study area (0-1000m, 30°S-30°N, 160°E-eastern coast) between 1958 and 2014 was evaluated for the first member of each model. We compared these trends to the oxygen content decadal variations induced by the PDO in the same region in the two models forced by past atmospheric conditions (NEMO, MOM6) and in the observation-based product.

2.4 Attribution of oxygen variability

We decompose oxygen variations (ΔO_2) into a thermal component tied to changes in solubility ($\Delta O_{2,sat}$) calculated using a python implementation of the TEOS-10 Gibbs SeaWater Oceanographic Toolbox (McDougall & Barker, 2011) and a non-thermal component tied to changes in circulation and biological activity (apparent oxygen utilization variation: ΔAOU):

$$\Delta O_2 = \Delta O_{2,sat} - \Delta AOU \tag{1}$$

We further decompose the non-thermal component ($-\Delta AOU$) into a large-scale transport term related to the renewal of oxygen by advective transport ($AdvTransport$) and a residual term containing the effects of biological activity and mixing ($BioMix$):

$$-\Delta AOU = AdvTransport + BioMix \tag{2}$$

162 We reconstructed advective transport offline using annual mean oxygen gradient
163 and velocity fields.

2.5 Identifying PDO signal

165 We used the monthly PDO index data distributed by NOAA (https://psl.noaa.gov/pdo/)
166 to track PDO phase changes. We retained decadal variations associated with the PDO
167 using a temporal butterworth low-pass filter with a cutoff period of 16 years that removes
168 high frequency variations associated with shorter variability modes such as ENSO (Fig-
169 ure S1). During the simulation period, the PDO index is characterized by two negative
170 phases (1958-1976 and 1998-2015) and a positive phase (1977-1997, Figure S1). Oxygen
171 fields (oxygen concentration, OMZ volume and oxygen budget terms) were filtered us-
172 ing the same approach to remove frequencies higher than 16 years and retain the signal
173 associated with the PDO .

3 Results

3.1 PDO control over tropical Pacific oxygen content and OMZ volume

176 The oxygen content in the upper tropical Pacific (0-1000m, 30°S-30°N, 160°E-eastern
177 coast) increases during PDO negative phases and decreases during positive phases in both
178 the NEMO and MOM6 simulations (solid lines in Figure 2a). We find that the oxygen
179 content is negatively correlated with the PDO index and varies by about -56.0 Tmol.decade.$^{-1}$°C^{-1}
180 in both models (slope of -5.66, r^2 = 0.56, p-value = 3.6×10^{-12} in NEMO; slope of -
181 55.6 Tmol.decade.$^{-1}$°C^{-1}, r^2 = 0.56, p-value= 5.6×10^{-12} in MOM6, Figure S2). On
182 average over the three PDO phases, the net change in oxygen amounted to ±29 Tmol.decade^{-1}
183 in NEMO and ±30.0 Tmol.decade^{-1} in MOM6 (Figure 2a), which correspond to changes
184 of ±0.30%.decade^{-1} and ±0.33%.decade^{-1} in total oxygen content. The two models sug-
185 gest, however, that the magnitude of the oxygen response to PDO varied in time, with
186 higher oxygenation rates found during the first negative phase (+38 and +35 Tmol.decade^{-1}
187 in NEMO and MOM6 between 1958 and 1976) compared to the most recent negative
188 phase (+22 and +29 Tmol.decade^{-1} between 1998 and 2015), and to the deoxygenation
189 rates found during the positive phase (-29 and -31 Tmol.decade^{-1} between 1977 and 1997,
190 Figure 2a).

191 We compare the simulated oxygen decadal variations to the observation-based data
192 product from Ito et al. (2017). Observations are sparse and only cover 39% of the trop-
193 ical Pacific volume, we therefore use oxygen concentrations instead of total oxygen con-
194 tent in this comparison (Figure 2c). The dataset shows a decadal oxygen variability of
195 ±0.9 umol.kg^{-1}.decade^{-1} in phase with the PDO, consisting of an average gain of +1.5
196 umol.kg^{-1}.decade^{-1} during the first negative phase and a loss of -1.1 umol.kg^{-1}.decade^{-1}
197 during the positive phase, but surprisingly stable oxygen concentrations during the last
198 negative phase (-0.01 umol.kg^{-1}.decade^{-1}, Fig. 2c). This later period is, however, the
199 least sampled, with on average 2034 observations per year versus 3525 per year for the
200 earlier period (Figure 2d). These observed oxygen changes are almost four times larger
201 than those simulated in the models (±0.25 umol.kg^{-1}.decade^{-1} in MOM6, and ±0.23
202 umol.kg^{-1}.decade^{-1} in NEMO). We assess the effect of heterogeneous sampling in space
203 and time by subsampling the simulated oxygen fields at the location of available obser-
204 vations (solid colored lines in Figure 2c). Once subsampled, the simulated oxygen changes
205 amplitude increases by a factor two during the first two PDO phases and is almost zero
206 during the last and least sampled period, improving the match with the data (Figure 2c,
207 r^2= 0.59 vs 0.18 in NEMO, r^2: 0.28 vs 0.19 in MOM6, Figure S2). The fact that the sub-
208 sampled models is well correlated with the data, but poorly with the full model results
209 (r^2= 0.04 in NEMO and 0.1 in MOM6, Figure S2) suggests that the data coverage is not
210 sufficient to capture the spatial and temporal variations associated with the PDO.

Decadal changes in oxygenation influence the simulated volume of the tropical Pacific OMZ which contracts during negative PDO phases and expands during positive phases (Figure 2b). In both models the rate of change in OMZ volume (defined here as [O2] < 45 umol.kg^{-1}) is similar, amounting to $\pm 1.3 \times 10^{14}$ m^3.decade^{-1} (corresponding to $\pm 0.37\%$.decade^{-1}) in NEMO and $\pm 1.5 \times 10^{14}$ m^3.decade^{-1} (± 0.27 %.decade^{-1}) in MOM6 (Figure 2b). Note that the tight link between PDO phases and OMZ volume rate of change shown here for the OMZ defined with an oxygen threshold of 45 umol.kg^{-1} (corresponding to a positive linear correlation: $+2.2 \times 10^{13}$ m^3.yr^{-1}.$^{\circ}$C^{-1}, r^2 = 0.40, p-value = 3.7×10^{-8} in NEMO and $+2.5 \times 10^{13}$ m^3.yr^{-1}.$^{\circ}$C^{-1}, r^2 = 0.43, p-value = 1.03×10^{-8} in MOM6, Figure S2) is robust and significant across all oxygen thresholds between 20 umol.kg^{-1} and 120 umol.kg^{-1} (Figure S3).

3.2 Key role of equatorial oxygen supply on decadal time-scales

In both simulations, decadal oxygen variations in the upper tropical Pacific are controlled by variations in advective transport (Figure 2e,f). Advective oxygen transport is stronger during negative phases and weaker during positive phases, resulting in an increase in oxygen content during negative phases and a decrease during positive phases, with change rates of ± 72 Tmol.decade^{-1} in NEMO and ± 83 Tmol.decade^{-1} in MOM6. Transport modulations also control surface nutrient supply and productivity, as well as subsurface organic carbon export and biological demand, and oxygen gradient changes alter mixing. Thus, changes in oxygen supply due to advective transport are offset up to 70% by changes in biological activity and mixing (± 49 and ± 61 Tmol.decade^{-1} in NEMO and MOM6 respectively, Figure 2e,f). Taken together, these non-thermal changes (advection, biology and mixing) represent variations ± 27 Tmol.decade^{-1} in NEMO and ± 29 Tmol.decade^{-1} that largely explain the net oxygen changes associated with PDO phases (± 29 Tmol.decade^{-1} and r^2 = 0.96 in NEMO, ± 30 Tmol.decade^{-1} and r^2 = 0.96 in MOM6). In contrast, solubility-induced changes in oxygen content are of a lower order of magnitude and show no significant correlation with PDO phases (Figure 2e,f, r^2=0.1 in NEMO and 0.04 in MOM6).

Over the simulation period, more than 70% of the oxygen supply by advective transport to the equatorial Pacific (0-1000m, 10°S-10°N, 160°E-Eastern coast) occurs between 2°S and 2°N (72% in NEMO and 79% in MOM6), and is sustained by the equatorial undercurrent (EUC) that transports subsurface oxygenated waters eastward (Figure 3a,b). The EUC supplies +387 Gmol.yr^{-1} in NEMO and +642 Gmol.yr^{-1} in MOM6 to the upper equatorial Pacific. On the other hand, the jets on either side of the equatorial undercurrent transport low oxygen waters westward (Figure 3a,b, -58 Gmol.yr^{-1} in NEMO and -79 Gmol.yr^{-1} in MOM6). These jets are better represented in MOM6 because of the higher horizontal resolution and lower numerical dissipation near the equator, which explains their higher impact on the oxygen budget. In both models, the oxygen transport by the equatorial undercurrent and the jets is modulated by 5-8% due to the changes in circulation associated with PDO phases. During PDO positive phase, the oxygen supply by the equatorial undercurrent weakens (-26 Gmol.yr^{-1}, -6.6% relative to the mean state in NEMO and -45 Gmol.yr^{-1}, -7.5% in MOM6), while during negative phases, the transport increases (+17 Gmol.yr^{-1}, +4.5% in NEMO and +34 Gmol.yr^{-1}, +5.6% in MOM6, Figure 3c-f).

Oxygen observations are too sparse to estimate decadal variations in oxygen transport. However, since the zonal subsurface oxygen gradient is a persistent feature of the equatorial Pacific, mass transport variability, which we can infer from the zonal velocity measured at the TAO moorings, is a good proxy for oxygen transport variability. On average over the TAO moorings measurement period (1988-present), the simulated EUC amplitude and westward shallowing following the thermocline are realistic compared to observations (Figure 3g-j, RMSE on climatological zonal velocities of 0.17 m.s^{-1} for NEMO and 0.12 m.s^{-1} for MOM6). For three of the four moorings (moorings at 190°E, 220°E

and 250°E), the zonal mass transport in the top 300 m is larger during the negative phases than the positive phase, as reproduced in the 2 simulations (Figure 3h-j). These results are also consistent with previous work (Kuntz & Schrag, 2021). In contrast, we see that the transport at the most western mooring (165°E) which does not measure the EUC core responds differently, with higher transport during the positive phase than negative phases (Figure 3g). We note that the models reproduce the sign of change expected from the observations but underestimate the amplitude of the variations up to a factor two (amplitudes of 4.4±4.3 % in observations vs. 1.3±1.7 % in NEMO and 1.9±2.5% in MOM6). This suggests that the mass transport decadal variability, and by extension the influence of PDO on the advective oxygen transport, might be underestimated by the models in the equatorial band.

4 Conclusion and discussion

Using two ocean general circulation biophysical simulations, we show that, during negative PDO phases, the upper tropical Pacific oxygen content increases by about 30 Tmol.decade^{-1}. The intensification of ocean currents in the upper tropical Pacific, in particular the equatorial undercurrent, increases the oxygen supply to the OMZ ($O_2 <45$ umol.kg^{-1}) leading to its contraction at a rate of 1.3×10^5 km^3.decade^{-1}. In contrast, during positive PDO phases, the supply by the equatorial undercurrent weakens, the oxygen content decreases and the OMZ expands by a similar amount (Figure 1b). Up to 70% of the oxygen variations tied to advective transport are offset by changes in biology and mixing. These results are consistent with velocity measurements from the TAO moorings and oxygen observations from Ito et al. (2017) available between 1958 and 2020 in the tropical Pacific. The key role of advective transport, biological demand and mixing is consistent with the work of Duteil et al. (2018), which suggested that oxygen changes in the equatorial suboxic zone (<20 umol.kg^{-1}) are controlled by advective processes. Here we identify a net change in the oxygen transport into the tropical Pacific subsurface in response to PDO phases. This is different from the east/west redistribution of oxygen in the upper layer (associated with the vertical movement of isopycnals during PDO phases) identified in Ito et al. (2019), which modulates the depth of the oxycline but has little influence on the volume of the tropical OMZ.

PDO-induced changes in oxygen estimated in this study using ocean models and observations are of the order of 0.25-0.90 umol.kg^{-1}.decade^{-1} (Fig4). The observation-based estimate is, however, about three times higher than that simulated by the two models (±0.90 umol.kg^{-1}.decade^{-1} vs. ±0.25 umol.kg^{-1}.decade^{-1}). Two factors contribute to this model-observation mismatch in the oxygen response. First, we find that data undersampling artificially amplifies oxygen decadal variability, as suggested by the larger variations obtained when subsampling the models similarly to observations compared to using the full model solution (from ±0.25 vs. ±0.40 umol.kg^{-1}.decade^{-1}, compare solid/dashed brown and green lines in Fig 4). Second, the two ocean models likely underestimate natural oxygen decadal variability. Indeed, the simulated variability in advective mass transport, which is a good indicator of oxygen transport, is only one third of that measured by the TAO buoys. However, we note that the model bias in advective transport would likely lead to a smaller oxygen bias (only half when comparing dashed lines in Fig4), because of the strong compensation between advective oxygen supply and biological demand in this region. The equatorial surface productivity and subsurface biological demand are tied to the ocean dynamics intensity supplying nutrients.

Changes in oxygen associated with the PDO are likely to obscure the anthropogenic deoxygenation trend and bias its estimates over the historical period (1958-2014). The oxygen concentration changes induced by the PDO estimated here (about ±0.25 umol.kg^{-1}.decade^{-1} in models and ±0.9 umol.kg^{-1}.decade^{-1} in observations, Fig4) are of the same order of magnitude as the deoxygenation trends estimated over a similar period using an ensemble of the latest generation of Earth system model (CMIP6) historical experiments (-0.2±0.2

umol.kg^{-1}.decade^{-1}, 1958-2014, Fig4), as well as the observation-based dataset of Ito and co-authors (-0.5 umol.kg^{-1}.decade^{-1}, 1958-2015, Fig4). Long-term human-driven oxygen loss and PDO-related oscillations in oxygen concentrations are therefore superimposed, and isolating them in the historical observations remains a challenge. Oxygen observations are sparse and require interpolations over large space-time domains which we show here introduce biases when inferring long-term trends in this region. In addition, most oxygen observations in the region were taken in the past 60 years which only covers 3 PDO cycles and limits the attribution of the trend to climate change. This is in line with Earth system models suggesting that the human-driven deoxygenation signal may only emerge in about 30 to 40 years in the tropical Pacific Ocean (Long et al., 2016; Schlunegger et al., 2019).

5 Acknowledgments

6 Open Research

Model data used to perform this analysis are available on zenodo (Currently on Zenodo Sandbox: `https://sandbox.zenodo.org/record/1129979`).
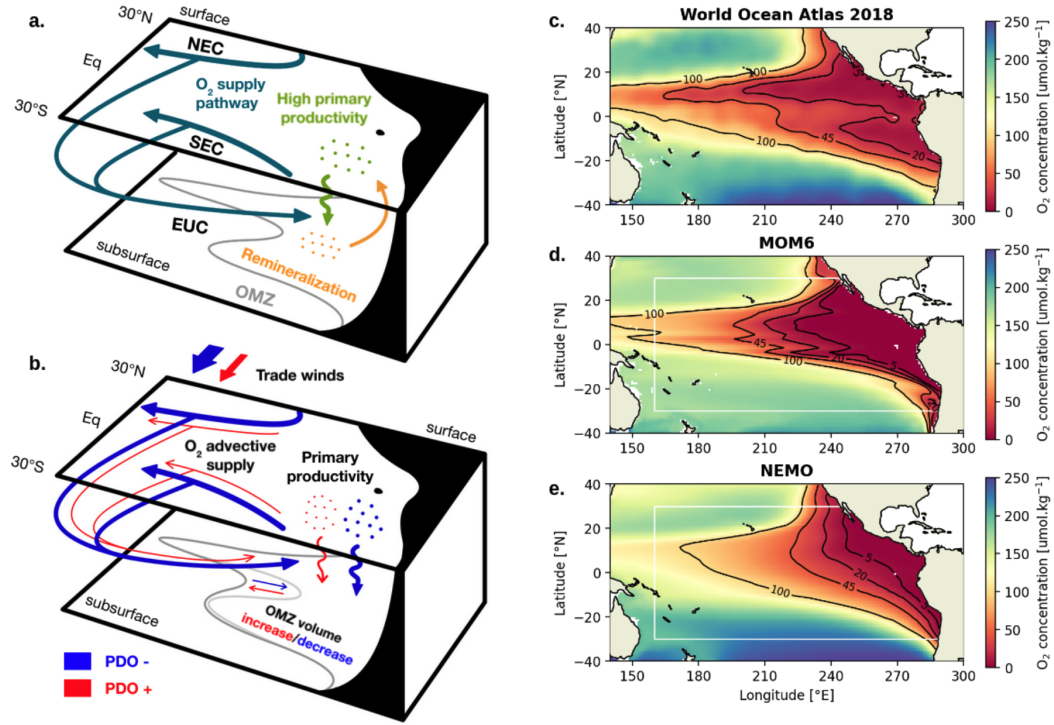
332 **7 Figures**

Figure 1. Biological processes and main ocean circulation pathways controlling the tropical Pacific Ocean OMZ (a) mean climatological state and (b) variability during PDO positive (red) and negative (blue) phases. NEC: north equatorial current, SEC: south equatorial current, EUC: equatorial undercurrent (adapted from Duteil et al. 2018 to reflect the results of current study). Oxygen concentration at 400 m in (c) the World Ocean Atlas 2018, (d) the MOM6 (1959-2020) and (e) NEMO (1958-2019) model simulations. Black lines correspond to oxygen iso-concentrations: 5, 20, 45, 100 umol.kg^{-1}. The white box in panels d-e delimits the study area.

Figure 2. Observed and modeled oxygen variability in the upper tropical Pacific (0-1000m, 30°S-30°N, 160°E-Eastern coast). Time series of a) oxygen content (in Tmol) and concentration (in umol.kg^{-1}) anomalies and b) OMZ volume anomaly in the MOM6 (brown) and NEMO (green) simulations. Time series of c) oxygen concentration anomaly time series in the Ito et al. (2017) data (black), and subsampled at the data location in the MOM6 (brown) and NEMO (green) simulations and d) amount of data for each year in the Ito et al. dataset. Changes in oxygen content (black), and contributions from changes in solubility (O2sat, red), advective transport (orange) and residual variations tied to biological activity and mixing (blue) in the e) MOM6 and f) NEMO simulations. In panels a-c and e-f, the thin dotted lines are the annual signals and the thick solid lines are the filtered decadal signals (obtained by applying a 16-years low pass filter on the annual signals). Blue and red shadings indicate periods of negative and positive PDO phases.
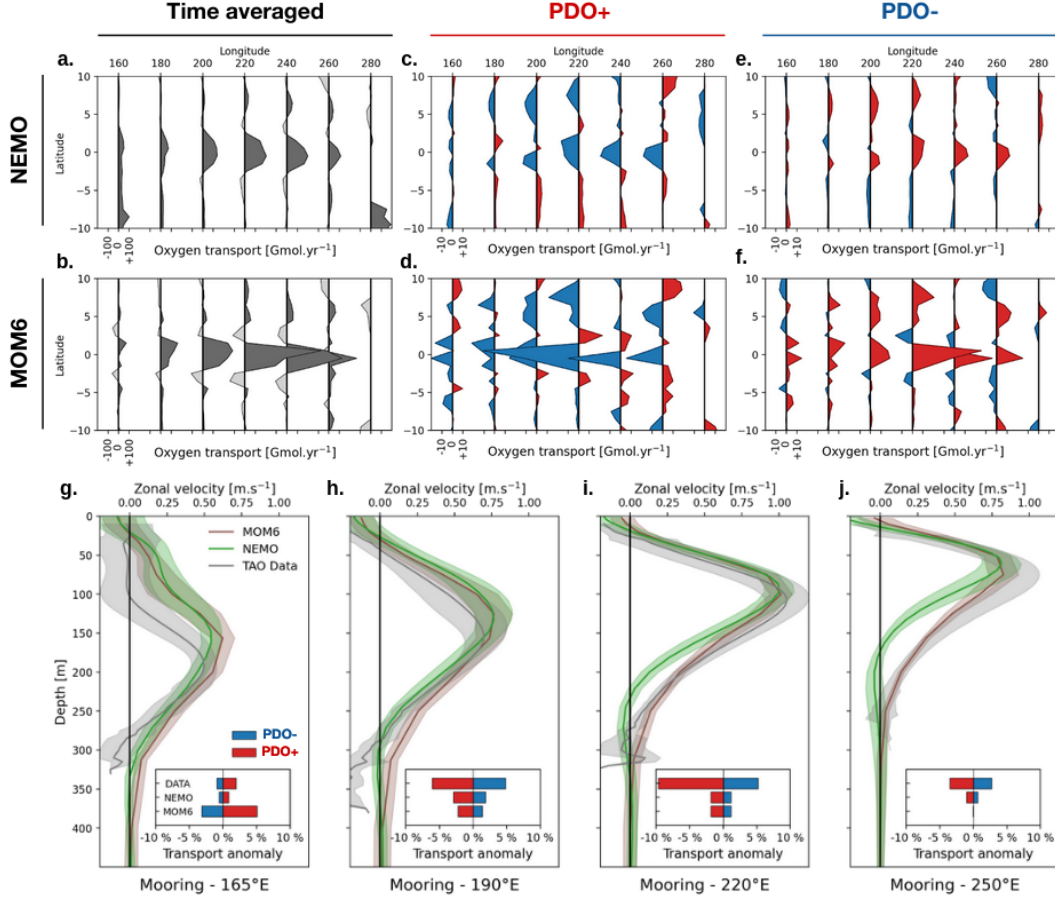
Figure 3. Zonal advective oxygen transport integrated over the top 1000m as a function of latitude in the NEMO (top row) and MOM6 (bottom row) models: (a,b) mean transport for the 1958-2020 period and anomalies relative to the mean state during (c,d) positive and (e,f) negative PDO phases. Positive transports are eastward. In panels c-f, red areas indicate an increase in oxygen supply by ocean currents while blue areas indicate a decrease. Model-data comparison for four equatorial Tropical Ocean Atmosphere (TAO) moorings located at (g) 165°E, (h) 190°E, (i) 220°E and (j) 250°E. Mean zonal velocity profiles (solid lines) and interannual variability (± 1 standard deviation indicated as shading) in the MOM6 simulation (brown), NEMO simulation (green) and TAO dataset (gray). For each panel, the insert is the transport anomaly integrated between 40 and 250m, relative to the mean state during positive (red) and negative (blue) PDO phases over the period covered by the TAO observations.
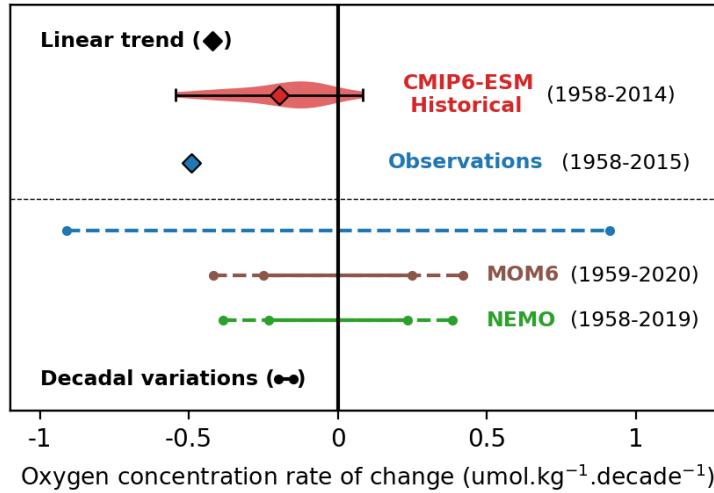
Figure 4. Mean oxygen concentration change rate (squares) in the upper tropical Pacific (0-1000m, 30°S-30°N, 160°E-Eastern Coast), in the observation-based product of Ito et al. (2017) (blue, 1958-2015) and in the CMIP6-ESM historical simulations (red, 1958-2014). The coloured area is the trend distributions for the different models. Decadal variations in mean oxygen concentration (lines) in the product of Ito et al. (blue), in the MOM6 (brown, 1959-2020) and NEMO (green, 1958-2019) simulations. The solid lines are the averaged decadal variation rates over the full basin, while the dashed lines is for a basin subsampled at locations where observations are available.

References

Adcroft, A., Anderson, W., Balaji, V., Blanton, C., Bushuk, M., Dufour, C. O., ... Zhang, R. (2019). The GFDL Global Ocean and Sea Ice Model OM4.0: Model Description and Simulation Features. *Journal of Advances in Modeling Earth Systems*, *11*(10), 3167–3211. Retrieved 2022-10-16, from `https://onlinelibrary.wiley.com/doi/abs/10.1029/2019MS001726` (_eprint: https://onlinelibrary.wiley.com/doi/pdf/10.1029/2019MS001726) doi: 10.1029/2019MS001726

Aumont, O., Ethé, C., Tagliabue, A., Bopp, L., & Gehlen, M. (2015, August). PISCES-v2: an ocean biogeochemical model for carbon and ecosystem studies. *Geoscientific Model Development*, *8*(8), 2465–2513. Retrieved 2022-10-16, from `https://gmd.copernicus.org/articles/8/2465/2015/` (Publisher: Copernicus GmbH) doi: 10.5194/gmd-8-2465-2015

Babbin, A. R., Bianchi, D., Jayakumar, A., & Ward, B. B. (2015, June). Rapid nitrous oxide cycling in the suboxic ocean. *Science*, *348*(6239), 1127–1129. Retrieved 2022-07-28, from `https://www.science.org/doi/full/10.1126/science.aaa8380` (Publisher: American Association for the Advancement of Science) doi: 10.1126/science.aaa8380

Bopp, L., Resplandy, L., Orr, J. C., Doney, S. C., Dunne, J. P., Gehlen, M., ... Vichi, M. (2013, October). Multiple stressors of ocean ecosystems in the 21st century: projections with CMIP5 models. *Biogeosciences*, *10*(10), 6225–6245. Retrieved 2022-10-16, from `https://bg.copernicus.org/articles/10/6225/2013/` (Publisher: Copernicus GmbH) doi: 10.5194/bg-10-6225-2013

Bopp, L., Resplandy, L., Untersee, A., Le Mezo, P., & Kageyama, M. (2017, September). Ocean (de)oxygenation from the Last Glacial Maximum to the twenty-first century: insights from Earth System models. *Philosoph-*

ical Transactions of the Royal Society A: Mathematical, Physical and Engineering Sciences, *375*(2102), 20160323. Retrieved 2022-10-16, from https://royalsocietypublishing.org/doi/full/10.1098/rsta.2016.0323 (Publisher: Royal Society) doi: 10.1098/rsta.2016.0323

Brandt, P., Bange, H. W., Banyte, D., Dengler, M., Didwischus, S.-H., Fischer, T., ... Visbeck, M. (2015, January). On the role of circulation and mixing in the ventilation of oxygen minimum zones with a focus on the eastern tropical North Atlantic. *Biogeosciences*, *12*(2), 489–512. Retrieved 2022-10-20, from https://bg.copernicus.org/articles/12/489/2015/ (Publisher: Copernicus GmbH) doi: 10.5194/bg-12-489-2015

Breitburg, D., Levin, L. A., Oschlies, A., Grégoire, M., Chavez, F. P., Conley, D. J., ... Zhang, J. (2018, January). Declining oxygen in the global ocean and coastal waters. *Science*, *359*(6371), eaam7240. Retrieved 2022-07-27, from https://www.science.org/doi/full/10.1126/science.aam7240 (Publisher: American Association for the Advancement of Science) doi: 10.1126/science.aam7240

Busecke, J. J. M., Resplandy, L., & Dunne, J. P. (2019). The Equatorial Undercurrent and the Oxygen Minimum Zone in the Pacific. *Geophysical Research Letters*, *46*(12), 6716–6725. Retrieved 2022-07-28, from https://onlinelibrary.wiley.com/doi/abs/10.1029/2019GL082692 (_eprint: https://onlinelibrary.wiley.com/doi/pdf/10.1029/2019GL082692) doi: 10.1029/2019GL082692

Deutsch, C., Berelson, W., Thunell, R., Weber, T., Tems, C., McManus, J., ... van Geen, A. (2014, August). Centennial changes in North Pacific anoxia linked to tropical trade winds. *Science*, *345*(6197), 665–668. Retrieved 2022-07-27, from https://www.science.org/doi/full/10.1126/science.1252332 (Publisher: American Association for the Advancement of Science) doi: 10.1126/science.1252332

Deutsch, C., Brix, H., Ito, T., Frenzel, H., & Thompson, L. (2011, July). Climate-Forced Variability of Ocean Hypoxia. *Science*, *333*(6040), 336–339. Retrieved 2022-07-27, from https://www.science.org/doi/full/10.1126/science.1202422 (Publisher: American Association for the Advancement of Science) doi: 10.1126/science.1202422

Duteil, O., Böning, C. W., & Oschlies, A. (2014). Variability in subtropical-tropical cells drives oxygen levels in the tropical Pacific Ocean. *Geophysical Research Letters*, *41*(24), 8926–8934. Retrieved 2022-07-28, from https://onlinelibrary.wiley.com/doi/abs/10.1002/2014GL061774 (_eprint: https://onlinelibrary.wiley.com/doi/pdf/10.1002/2014GL061774) doi: 10.1002/2014GL061774

Duteil, O., Oschlies, A., & Böning, C. W. (2018, November). Pacific Decadal Oscillation and recent oxygen decline in the eastern tropical Pacific Ocean. *Biogeosciences*, *15*(23), 7111–7126. Retrieved 2022-07-27, from https://bg.copernicus.org/articles/15/7111/2018/ (Publisher: Copernicus GmbH) doi: 10.5194/bg-15-7111-2018

Eyring, V., Bony, S., Meehl, G. A., Senior, C. A., Stevens, B., Stouffer, R. J., & Taylor, K. E. (2016, May). Overview of the Coupled Model Intercomparison Project Phase 6 (CMIP6) experimental design and organization. *Geoscientific Model Development*, *9*(5), 1937–1958. Retrieved 2022-11-11, from https://gmd.copernicus.org/articles/9/1937/2016/ (Publisher: Copernicus GmbH) doi: 10.5194/gmd-9-1937-2016

Friedlingstein, P., O'Sullivan, M., Jones, M. W., Andrew, R. M., Hauck, J., Olsen, A., ... Zaehle, S. (2020, December). Global Carbon Budget 2020. *Earth System Science Data*, *12*(4), 3269–3340. Retrieved 2022-10-16, from https://essd.copernicus.org/articles/12/3269/2020/ (Publisher: Copernicus GmbH) doi: 10.5194/essd-12-3269-2020

Garcia, H., Boyer, T., Baranova, O., Locarnini, R., Mishonov, A., Grodsky, A. e., . . . others (2019). World ocean atlas 2018: Product documentation. *A. Mishonov, Technical Editor*, *1*, 1–20.

Helm, K. P., Bindoff, N. L., & Church, J. A. (2011). Observed decreases in oxygen content of the global ocean. *Geophysical Research Letters*, *38*(23). Retrieved 2022-10-16, from `https://onlinelibrary.wiley.com/doi/abs/10.1029/2011GL049513` (_eprint: https://onlinelibrary.wiley.com/doi/pdf/10.1029/2011GL049513) doi: 10.1029/2011GL049513

Hong, L., Zhang, L., Chen, Z., & Wu, L. (2014). Linkage between the Pacific Decadal Oscillation and the low frequency variability of the Pacific Subtropical Cell. *Journal of Geophysical Research: Oceans*, *119*(6), 3464–3477. Retrieved 2022-07-28, from `https://onlinelibrary.wiley.com/doi/abs/10.1002/2013JC009650` (_eprint: https://onlinelibrary.wiley.com/doi/pdf/10.1002/2013JC009650) doi: 10.1002/2013JC009650

Ito, T., & Deutsch, C. (2010). A conceptual model for the temporal spectrum of oceanic oxygen variability. *Geophysical Research Letters*, *37*(3). Retrieved 2022-07-27, from `https://onlinelibrary.wiley.com/doi/abs/10.1029/2009GL041595` (_eprint: https://onlinelibrary.wiley.com/doi/pdf/10.1029/2009GL041595) doi: 10.1029/2009GL041595

Ito, T., Long, M. C., Deutsch, C., Minobe, S., & Sun, D. (2019). Mechanisms of Low-Frequency Oxygen Variability in the North Pacific. *Global Biogeochemical Cycles*, *33*(2), 110–124. Retrieved 2022-07-27, from `https://onlinelibrary.wiley.com/doi/abs/10.1029/2018GB005987` (_eprint: https://onlinelibrary.wiley.com/doi/pdf/10.1029/2018GB005987) doi: 10.1029/2018GB005987

Ito, T., Minobe, S., Long, M. C., & Deutsch, C. (2017). Upper ocean O2 trends: 1958–2015. *Geophysical Research Letters*, *44*(9), 4214–4223. Retrieved 2022-10-16, from `https://onlinelibrary.wiley.com/doi/abs/10.1002/2017GL073613` (_eprint: https://onlinelibrary.wiley.com/doi/pdf/10.1002/2017GL073613) doi: 10.1002/2017GL073613

Keeling, R. F., Körtzinger, A., & Gruber, N. (2010). Ocean Deoxygenation in a Warming World. *Annual Review of Marine Science*, *2*(1), 199–229. Retrieved 2022-10-16, from `https://doi.org/10.1146/annurev.marine.010908.163855` (_eprint: https://doi.org/10.1146/annurev.marine.010908.163855) doi: 10.1146/annurev.marine.010908.163855

Kuntz, L. B., & Schrag, D. P. (2021, March). Subtropical modulation of the equatorial undercurrent: a mechanism of Pacific variability. *Climate Dynamics*, *56*(5), 1937–1949. Retrieved 2022-11-03, from `https://doi.org/10.1007/s00382-020-05568-w` doi: 10.1007/s00382-020-05568-w

Kwiatkowski, L., Torres, O., Bopp, L., Aumont, O., Chamberlain, M., Christian, J. R., . . . Ziehn, T. (2020, July). Twenty-first century ocean warming, acidification, deoxygenation, and upper-ocean nutrient and primary production decline from CMIP6 model projections. *Biogeosciences*, *17*(13), 3439–3470. Retrieved 2022-10-16, from `https://bg.copernicus.org/articles/17/3439/2020/` (Publisher: Copernicus GmbH) doi: 10.5194/bg-17-3439-2020

Levin, L. A. (2018). Manifestation, Drivers, and Emergence of Open Ocean Deoxygenation. *Annual Review of Marine Science*, *10*(1), 229–260. Retrieved 2022-10-16, from `https://doi.org/10.1146/annurev-marine-121916-063359` (_eprint: https://doi.org/10.1146/annurev-marine-121916-063359) doi: 10.1146/annurev-marine-121916-063359

Liao, E., Resplandy, L., Liu, J., & Bowman, K. W. (2020). Amplification

of the Ocean Carbon Sink During El Niños: Role of Poleward Ekman Transport and Influence on Atmospheric CO2. *Global Biogeochemical Cycles*, *34*(9), e2020GB006574. Retrieved 2022-10-16, from `https://onlinelibrary.wiley.com/doi/abs/10.1029/2020GB006574` (_eprint: https://onlinelibrary.wiley.com/doi/pdf/10.1029/2020GB006574) doi: 10.1029/2020GB006574

Long, M. C., Deutsch, C., & Ito, T. (2016). Finding forced trends in oceanic oxygen. *Global Biogeochemical Cycles*, *30*(2), 381–397. Retrieved 2022-10-16, from `https://onlinelibrary.wiley.com/doi/abs/10.1002/2015GB005310` (_eprint: https://onlinelibrary.wiley.com/doi/pdf/10.1002/2015GB005310) doi: 10.1002/2015GB005310

Madec, G., Bourdallé-Badie, R., Bouttier, P.-A., Bricaud, C., Bruciaferri, D., Calvert, D., . . . Vancoppenolle, M. (2017, October). *NEMO ocean engine* (report). Retrieved 2022-10-16, from `https://www.earth-prints.org/handle/2122/13309` (Accepted: 2020-02-27T08:10:54Z) doi: 10.5281/zenodo.3248739

Mantua, N. J., Hare, S. R., Zhang, Y., Wallace, J. M., & Francis, R. C. (1997, June). A Pacific Interdecadal Climate Oscillation with Impacts on Salmon Production*. *Bulletin of the American Meteorological Society*, *78*(6), 1069–1080. Retrieved 2022-08-13, from `https://journals.ametsoc.org/view/journals/bams/78/6/1520-0477_1997_078_1069_apicow_2_0_co_2.xml` (Publisher: American Meteorological Society Section: Bulletin of the American Meteorological Society) doi: 10.1175/1520-0477(1997)078⟨1069:APICOW⟩2.0.CO;2

McDougall, T., & Barker, P. (2011). Getting started with TEOS-10 and the Gibbs Seawater (GSW) oceanographic toolbox. *Scor/Iapso WG*, *127*, 1–28.

Oschlies, A., Duteil, O., Getzlaff, J., Koeve, W., Landolfi, A., & Schmidtko, S. (2017, September). Patterns of deoxygenation: sensitivity to natural and anthropogenic drivers. *Philosophical Transactions of the Royal Society A: Mathematical, Physical and Engineering Sciences*, *375*(2102), 20160325. Retrieved 2022-10-16, from `https://royalsocietypublishing.org/doi/full/10.1098/rsta.2016.0325` (Publisher: Royal Society) doi: 10.1098/rsta.2016.0325

Schlunegger, S., Rodgers, K. B., Sarmiento, J. L., Frölicher, T. L., Dunne, J. P., Ishii, M., & Slater, R. (2019, September). Emergence of anthropogenic signals in the ocean carbon cycle. *Nature Climate Change*, *9*(9), 719–725. Retrieved 2022-08-13, from `https://www.nature.com/articles/s41558-019-0553-2` (Number: 9 Publisher: Nature Publishing Group) doi: 10.1038/s41558-019-0553-2

Schmidtko, S., Stramma, L., & Visbeck, M. (2017, February). Decline in global oceanic oxygen content during the past five decades. *Nature*, *542*(7641), 335–339. Retrieved 2022-10-16, from `https://www.nature.com/articles/nature21399` (Number: 7641 Publisher: Nature Publishing Group) doi: 10.1038/nature21399

Stock, C. A., Dunne, J. P., Fan, S., Ginoux, P., John, J., Krasting, J. P., . . . Zadeh, N. (2020). Ocean Biogeochemistry in GFDL's Earth System Model 4.1 and Its Response to Increasing Atmospheric CO2. *Journal of Advances in Modeling Earth Systems*, *12*(10), e2019MS002043. Retrieved 2022-10-16, from `https://onlinelibrary.wiley.com/doi/abs/10.1029/2019MS002043` (_eprint: https://onlinelibrary.wiley.com/doi/pdf/10.1029/2019MS002043) doi: 10.1029/2019MS002043

Stramma, L., Johnson, G. C., Sprintall, J., & Mohrholz, V. (2008, May). Expanding Oxygen-Minimum Zones in the Tropical Oceans. *Science*, *320*(5876), 655–658. Retrieved 2022-07-27, from `https://www.science.org/doi/full/10.1126/science.1153847` (Publisher: American Association for the Advancement of Science) doi: 10.1126/science.1153847

Stramma, L., Prince, E. D., Schmidtko, S., Luo, J., Hoolihan, J. P., Visbeck, M.,

⁵²⁴ . . . Körtzinger, A. (2012, January). Expansion of oxygen minimum zones
⁵²⁵ may reduce available habitat for tropical pelagic fishes. *Nature Climate*
⁵²⁶ *Change*, *2*(1), 33–37. Retrieved 2022-10-16, from https://www.nature.com/
⁵²⁷ articles/nclimate1304 (Number: 1 Publisher: Nature Publishing Group)
⁵²⁸ doi: 10.1038/nclimate1304
⁵²⁹ Stramma, L., Schmidtko, S., Levin, L. A., & Johnson, G. C. (2010, April). Ocean
⁵³⁰ oxygen minima expansions and their biological impacts. *Deep Sea Re-*
⁵³¹ *search Part I: Oceanographic Research Papers*, *57*(4), 587–595. Retrieved
⁵³² 2022-07-27, from https://linkinghub.elsevier.com/retrieve/pii/
⁵³³ S0967063710000294 doi: 10.1016/j.dsr.2010.01.005
⁵³⁴ Tsujino, H., Urakawa, S., Nakano, H., Small, R. J., Kim, W. M., Yeager, S. G., . . .
⁵³⁵ Yamazaki, D. (2018, October). JRA-55 based surface dataset for driving
⁵³⁶ ocean–sea-ice models (JRA55-do). *Ocean Modelling*, *130*, 79–139. Retrieved
⁵³⁷ 2022-10-16, from https://www.sciencedirect.com/science/article/pii/
⁵³⁸ S146350031830235X doi: 10.1016/j.ocemod.2018.07.002
⁵³⁹ Vaquer-Sunyer, R., & Duarte, C. M. (2008, October). Thresholds of hypoxia
⁵⁴⁰ for marine biodiversity. *Proceedings of the National Academy of Sciences*,
⁵⁴¹ *105*(40), 15452–15457. Retrieved 2022-07-28, from https://www.pnas.org/
⁵⁴² doi/10.1073/pnas.0803833105 (Publisher: Proceedings of the National
⁵⁴³ Academy of Sciences) doi: 10.1073/pnas.0803833105
⁵⁴⁴ Yang, S., Chang, B. X., Warner, M. J., Weber, T. S., Bourbonnais, A. M., Santoro,
⁵⁴⁵ A. E., . . . Bianchi, D. (2020, June). Global reconstruction reduces the un-
⁵⁴⁶ certainty of oceanic nitrous oxide emissions and reveals a vigorous seasonal
⁵⁴⁷ cycle. *Proceedings of the National Academy of Sciences*, *117*(22), 11954–
⁵⁴⁸ 11960. Retrieved 2022-08-05, from https://www.pnas.org/doi/abs/10.1073/
⁵⁴⁹ pnas.1921914117 (Publisher: Proceedings of the National Academy of Sci-
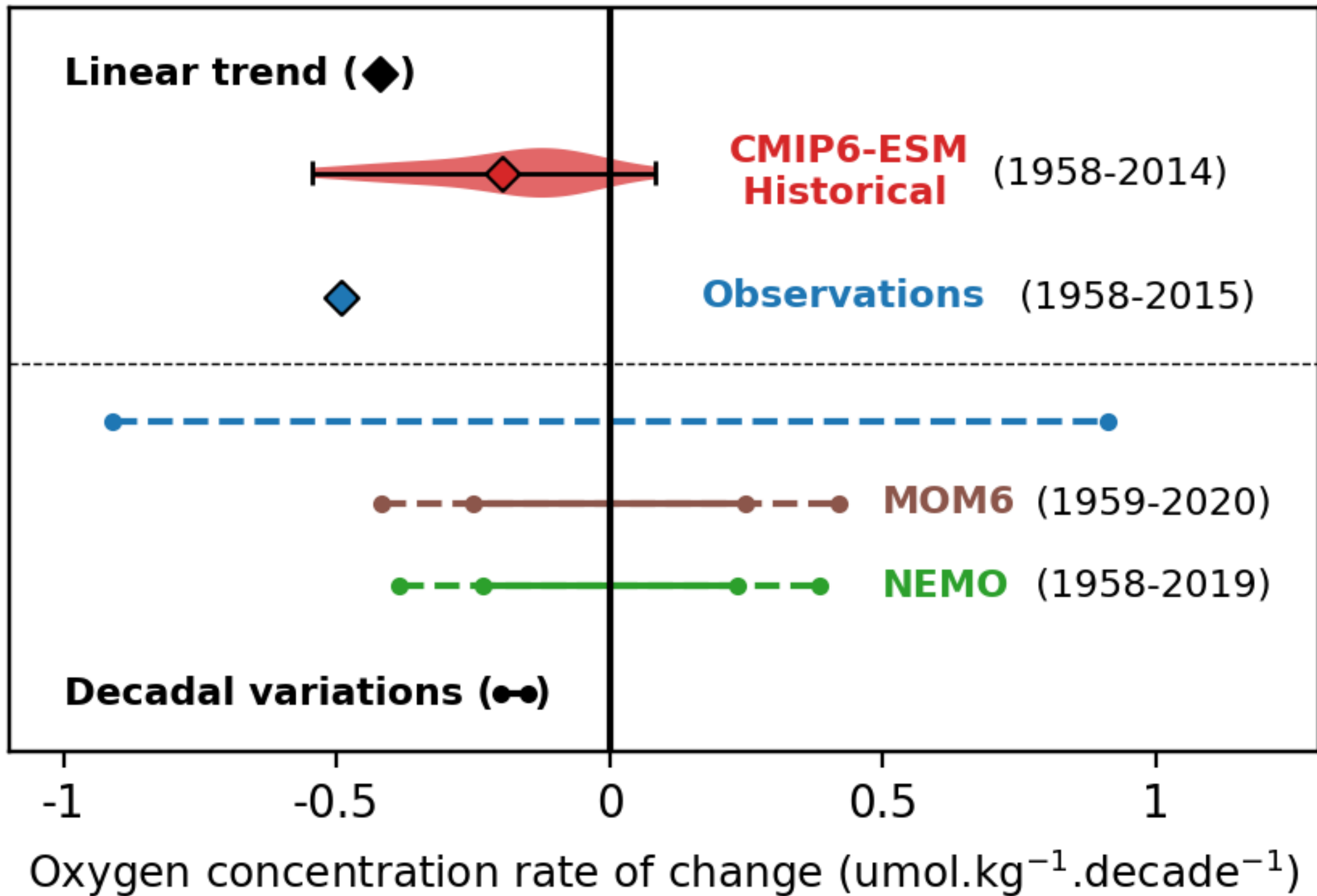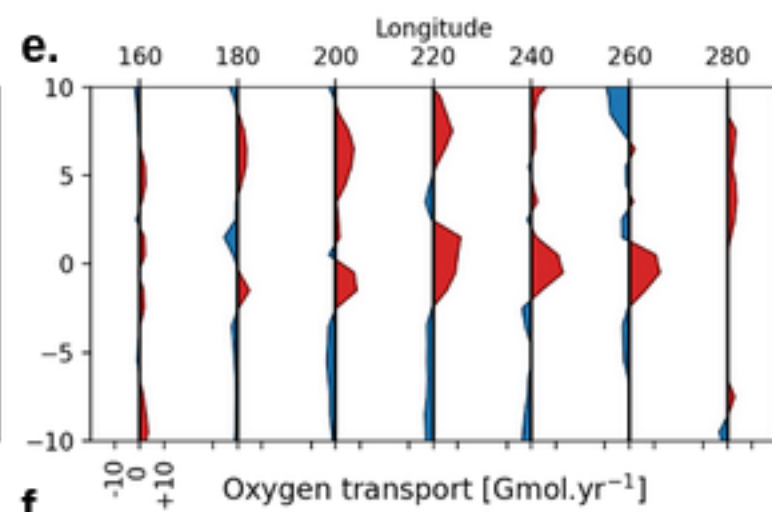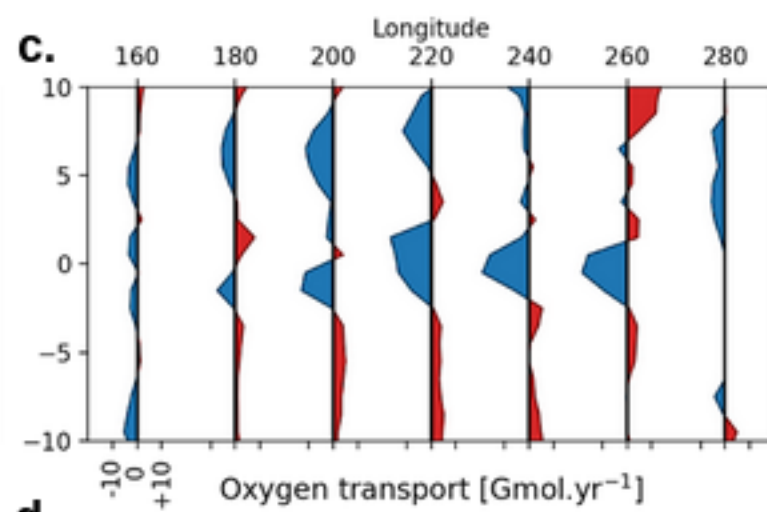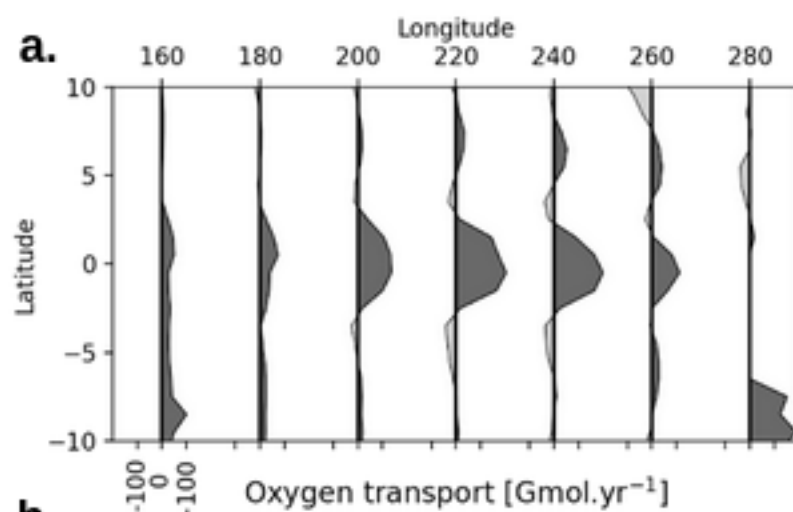⁵⁵⁰ ences) doi: 10.1073/pnas.1921914117

Figure 4.

Linear trend (◆)

CMIP6-ESM Historical (1958-2014)

Observations (1958-2015)

MOM6 (1959-2020)

NEMO (1958-2019)

Decadal variations (●━●)

Oxygen concentration rate of change (umol.kg^{-1}.decade^{-1})

Figure 3.

Time averaged | PDO+ | PDO-

a. NEMO — Longitude: 160 180 200 220 240 260 280 — Latitude 10 to −10 — Oxygen transport [Gmol.yr⁻¹]: −100 0 +100

b. MOM6 — Oxygen transport [Gmol.yr⁻¹]: −100 0 +100

c. NEMO — Longitude: 160 180 200 220 240 260 280 — Oxygen transport [Gmol.yr⁻¹]: −10 0 +10

d. MOM6 — Oxygen transport [Gmol.yr⁻¹]: −10 0 +10

e. NEMO — Longitude: 160 180 200 220 240 260 280 — Oxygen transport [Gmol.yr⁻¹]: −10 0 +10

f. MOM6 — Oxygen transport [Gmol.yr⁻¹]: −10 0 +10

g. Zonal velocity [m.s⁻¹]: 0.00 0.25 0.50 0.75 1.00 — Depth [m]: 0 to 400 — MOM6, NEMO, TAO Data — PDO−, PDO+ — Transport anomaly: −10 % −5 % 0 % 5 % 10 % (DATA, NEMO, MOM6) — Mooring - 165°E

h. Zonal velocity [m.s⁻¹]: 0.00 0.25 0.50 0.75 1.00 — Transport anomaly: −10 % −5 % 0 % 5 % 10 % — Mooring - 190°E

i. Zonal velocity [m.s⁻¹]: 0.00 0.25 0.50 0.75 1.00 — Transport anomaly: −10 % −5 % 0 % 5 % 10 % — Mooring - 220°E

j. Zonal velocity [m.s⁻¹]: 0.00 0.25 0.50 0.75 1.00 — Transport anomaly: −10 % −5 % 0 % 5 % 10 % — Mooring - 250°E

Figure 2.

Figure 1.